Near-field radiative transfer by bulk hyperbolic polaritons across vacuum gap

Hakan Salihoglu, Xianfan Xu*

School of Mechanical Engineering and Birck Nanotechnology Center, Purdue University, West Lafayette, IN 47907, USA

ARTICLE INFO

ABSTRACT

Thermal radiation has always been treated as a surface phenomenon. A recent study has demonstrated that new radiation channels, the hyperbolic phonon polaritons, can contribute to heat transfer inside bulk hyperbolic materials with a heat flux comparable to conduction. For near-field radiative transfer across a vacuum gap between two hyperbolic materials, hyperbolic phonon polaritons have been considered as surface modes that are responsible for heat transfer enhancement. Here, we analyze near-field radiative transfer due to hyperbolic phonon polaritons, driven by temperature gradient inside the bulk materials. We develop a mesoscale many-body scattering approach to account for the role of hyperbolic phonon polaritons in radiative transfer in the bulk and across a vacuum gap. Our study points out the equivalency between the bulk-generated mode and the surface mode in the absence of a temperature gradient in the material, and hence provide a unified framework for near-field radiative transfer by hyperbolic phonon polaritons. The results also elucidate contributions of the bulk-generated mode and the bulk temperature profile in the enhanced near-field radiative transfer.

© 2021 Elsevier Ltd. All rights reserved.

1. Introduction

Planck's law predicts blackbody radiation by an object at finite temperatures [1]. For longer than decades, blackbody radiation has been considered the theoretical limit of thermal radiation. Recent theoretical studies [2–6] have shown that thermal radiation exceeds blackbody radiation, with greatly enhanced radiative transfer when two objects are positioned within a near-field regime (at a wavelength $< 10~\mu$m at room temperature). Experimental studies [7–15] have verified such predictions. Enhanced near-field thermal radiation results in numerous possible emerging technologies [16–20]. Near-field radiation enhancement occurs between several types of materials arising from coupling of surface waves that propagate along the vacuum-material interface such as surface plasmon polaritons (SPP) in metals and surface phonon polaritons (SPhP) in polar dielectrics [7,21–25]. Computationally, the contribution of surface polaritons in near-field radiation has been incorporated into a two-body formalism [6]. The two-body formalism, which is also called Polder and van Hove formalism [26], considers all radiation modes that lead energy transport across the separation are generated at the surface based on surface temper-

atures. Another type of materials that have been investigated for enhancing near-field radiative transfer is hyperbolic materials [27–32], which have already been shown to have promising applications including broadband-enhanced spontaneous emission [33,34], hyperbolic lensing [35,36], and near-perfect absorption [37]. Hyperbolic materials possess opposite signs of dielectric components along two orthogonal principal axes within certain wavelength bands called Reststrahlen bands, and support bulk propagating modes called hyperbolic phonon polaritons (HPhP) [38,39]. HPhP can attain very high wave vector κ, therefore, they are also referred to as high-κ modes. These high-κ modes are confined and deeply sub-diffraction [40,41]. So far, contribution of HPhP modes to near-field radiative heat transfer has been analyzed as surface modes using the two body formalism [42,43].

Radiation can also be emitted from a surface that has a temperature gradient into the surface. Moreover, our recent study has shown, in a hyperbolic material, a temperature gradient can drive radiation inside the hyperbolic material due to the large amount of the propagating bulk HPhP modes. Importantly, this radiation heat flux can be comparable to phonon conduction [44]. The purpose of this study is to understand the physical process of near-field radiation arising from HPhPs, driven by a temperature gradient inside hyperbolic materials. We use a many-body approach to consider radiation from a non-uniform body and across a vacuum gap. Several studies have implemented this method to study near-field radiation, for example, to take into account carrier concentra-

---

* Corresponding author.
E-mail address: xxu@ecn.purdue.edu (X. Xu).

Nomenclature

c	speed of light in vacuum, m/s
d	vacuum separation, m
$\boldsymbol{E}$	electric field vector, m.kg/(s³.A)
h	heat transfer or coupling coefficient, W/m² K
i	$\sqrt{-1}$, [-]
Im	imaginary part of a variable, [-]
k_i	wave vector component in i direction, 1/m
k_B	Boltzmann constant, $1.38064852 \times 10^{-23}$ J/K
k_o	wave vector in vacuum, 1/m
N	total number of slabs, [-]
$q^{(j)}$	net radiative heat transfer into slab j, W/m²
$q_{j,\gamma}$	net radiative heat exchange between slabs j and γ, W/m²
$q_{j\rightarrow\gamma}$	radiative heat transfer from slab j to γ, W/m²
r	Fresnel reflection coefficient, [-]
Re	real part of a variable, [-]
S_z	z component of Poynting vector, W/(m² rad/s)
T_j	temperature of slab j, K
$\mathcal{T}^{j,\gamma}$	energy exchange function between slab j and γ, [-]
x,y,z	cartesian coordinates, m
z_j	position of boundary j, m
$\hat{x},\hat{y},\hat{z}$	unit vectors in corresponding directions, [-]

Greek symbols

β	parameter combining material property and wave vector as defined in S4, [-]
ε_{xy}	xy component of dielectric tensor, [-]
θ	mean energy, J
g_{Exy}	xy component of the Weyl tensor for electric field, m
$\hbar$	reduced Planck constant, $1.054571800 \times 10^{-34}$ J s
κ	parallel wave vector component, 1/m
$\tau_{j\rightarrow\gamma}$	transmission coefficient through slabs from j to γ, [-]
φ	transmission across vacuum gap in many-body system, [-]
ω	angular frequency, rad/s
δ	slab thickness, m

Subscripts/superscripts

C	cold side
H	hot side
j	index of emitter
m	index of slab next to vacuum
p	p polarization
q	polarization state (s,p)
s	s polarization
γ	index of receiver

tion gradient [45] or layered material structures [46,47]. Our study shows that HPhPs as bulk-originated modes are a general representation for near-field thermal radiation across a vacuum gap. In the absence of temperature gradient, near-field radiation caused by the surface mode is simply a special case, as the underlying contributing energy carriers are the same HPhPs in the Reststrahlen bands. Our study also elucidates the detailed processes of propagation of HPhPs across a vacuum gap and their contribution to near-field radiative transfer in the presence of temperature gradients in the material.

2. Theoretical framework

2.1. Near-field radiative transfer for two-body system with uniform temperature

We start our discussion with a brief review of the two-body PvH formalism. We consider two planar continuous media, each at a uniform temperature and separated by a vacuum gap, d, along the z axis ($\perp$) and in contact with hot and cold reservoirs at T_H and T_C, respectively, in the x-y plane ($\parallel$). Hot (1) and cold (2) media are at reservoir temperatures, $T_1 = T_H$ and $T_2 = T_C$, respectively. Heat flux (the net radiative heat transfer) from medium 1 to 2 reads: [26]

$$q^{(2)} = -q^{(1)} = \int_0^\infty \frac{d\omega}{2\pi}[\Theta(\omega,T_1) - \Theta(\omega,T_2)] \int_{\omega/c}^{\kappa_{max}} \frac{d\kappa}{2\pi}\kappa \sum_{i=s,p} \mathcal{T}_q^{1,2} \quad (1)$$

$\Theta(\omega,T)$ is mean energy of Planck oscillators with frequency ω at temperature T, and is given by $\hbar\omega/(e^{\hbar\omega/k_BT}-1)$, where $\hbar$ and k_B are the reduced Planck constant and Boltzmann constant, respectively. κ denotes the wave vector component parallel to planar surface ($k = \kappa + k_z\hat{z} = k_x\hat{x} + k_y\hat{y} + k_z\hat{z}$, where $\hat{x}$ is unit vector in x direction). Since the contribution from propagating waves in vacuum ($\kappa < \omega/c$, where ω/c is modulus of wave vector in vacuum) is negligible for near-field regime of interest, we only consider the contribution of evanescent waves in vacuum ($\kappa > \omega/c$). Each mode represented by κ corresponds to a channel that energy can flow through. Energy transmission across the vacuum gap by a mode is expressed by an energy exchange function, $\mathcal{T}_q^{1,2}$, as: [26]

$$\mathcal{T}_q^{1,2} = \frac{4Im(r_1^q)Im(r_2^q)e^{-2Im(k_{z,o})d}}{\left|1 - r_1^q r_2^q e^{2ik_{z,o}d}\right|^2} \quad (2)$$

$\mathcal{T}_q^{1,2}$ represents the fraction of energy across the vacuum gap and is equal to or smaller than 1. The exponential term cuts off contributions from modes with wave vectors $Im(k_{z,o}) \gg d^{-1}$. For waves supported at resonant frequencies, $|1 - r_1^q r_2^q e^{2ik_{z,o}d}|^2$ becomes very small and compensates for the exponential decay of waves. In this case, $\mathcal{T}_q^{1,2}$ approaches unity.

Thermal radiation is transferred in the form of electromagnetic energy, and derivation of the energy transfer relies on the expression of thermal radiation, the ensemble averaged Poynting vector $\langle \boldsymbol{S}(z,\omega,T)\rangle_z$ from medium 1 at temperature T to an observation point z in medium 2: [22]

$$\langle S(z,\omega,T)\rangle_z = \frac{\omega^2}{c^2}\frac{\Theta(\omega,T)}{\pi^2}Re\left\{i\int_{z'}dz'\int_{\omega/c}^{\kappa_{max}}d\kappa\kappa\left(g_{Ex\alpha}\varepsilon''_{\alpha\alpha}g^*_{Hy\alpha} - g^*_{Hx\alpha}\varepsilon''_{\alpha\alpha}g_{Ey\alpha}\right)\right\} \quad (3)$$

Repeating indices are summed, and index α represents an orthogonal component (x, y, z). Subscript z indicates the z component of Poynting vector, c is speed of light in vacuum and $\varepsilon''_{\alpha\alpha}$ is the imaginary part of diagonal component of dielectric tensor. z' represents the coordinate, and integration over z' is performed for medium 1. $g_{Ex\alpha}$ and $g_{Hy\alpha}$ are the Weyl components of dyadic Green tensor of electric and magnetic fields, respectively [22]. The Weyl tensor for the electric field is given as

$$\overset{\leftrightarrow}{g}_E(\kappa,z,z',\omega) = \frac{i}{2}\frac{1}{k_{z,1}^q}\sum_{q=p,s}\tau_{1\rightarrow2}^q \mathbf{E}_q(z,\kappa) \otimes \mathbf{E}_q(z',\kappa) \quad (4)$$

The Weyl components relate a source point in medium 1 with an observation point in medium 2 via the transmission from medium 1 to 2 across the vacuum gap, $\tau_{1\rightarrow2}^q$. $\otimes$ represents tensor product. $\mathbf{E}_q(z',\kappa)$ is right going wave at $z = 0$ (the interface of the hot medium) originated from unit strength wave at z' in
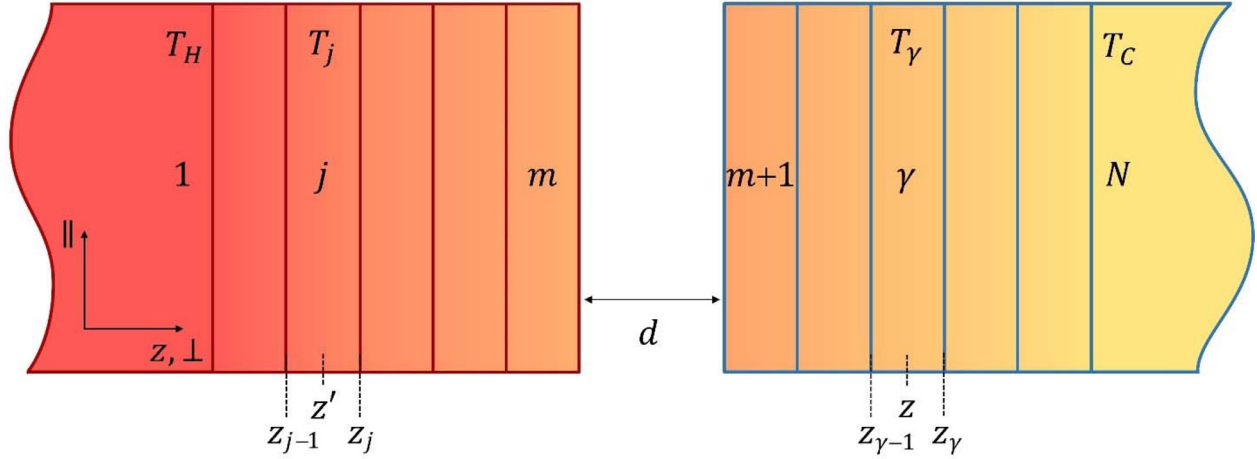
Fig. 1. Many-body system of two semi-infinite media with temperature gradient. Slabs extend to infinity in the in-plane ∥ direction (x,y plane). The global system consists of N-bodies or slabs, and slabs 1 and N correspond to hot and cold reservoirs at constant temperatures T_H and T_C, respectively. Undergoing radiative heat exchange, intermediate slabs reach their local equilibrium temperature, T_j. The region between two media is the vacuum gap with separation d. Position of slabs j and γ represented here corresponds to the second scenario.

medium 1, and $\boldsymbol{E}_q(z, \kappa)$ is wave at z in medium 2 originated from unit strength wave at d (the interface of the cold medium):

$$\boldsymbol{E}_q(z', \kappa) = \boldsymbol{e}_{q+} e^{-ik_{z,1}^q z'} \tag{5}$$

$$\boldsymbol{E}_q(z, \kappa) = \boldsymbol{e}_{q+} e^{ik_{z,2}^q (z-d)} \tag{6}$$

$\boldsymbol{e}_{q+}$ is the polarization vector for waves propagating to the right direction (+). $\tau_{1\to2}^q$ and the expressions for the terms in Eqs. (5) and (6) are given in Supplemental Material S1. Procedures for finding the Weyl components for magnetic fields are also given in Supplemental Material S1. To find the total radiative energy from medium 1 to 2, the Poynting vector is evaluated at the surface of medium 2 ($z = d$) and infinity. The difference of these Poynting vectors yield the total radiative energy from medium 1 to 2. The procedure is repeated for that from medium 2 to 1, and the difference of the two is the net radiative heat flux expressed in Eq. (1).

2.2. Near-field radiative transfer for many-body system with nonuniform temperature

To account for the temperature gradient in the media, we use a many-body scattering method as shown in Fig. 1. The global system consists of N bodies or slabs (slabs 1 and N are hot and cold reservoirs, respectively), and each slab, labeled with j, γ, or m in Fig. 1 is at a local equilibrium temperature. We consider a uniaxial material with out-of-plane component ($\perp$) lying along the z axis, and in-plane components ($\parallel$) within the invariant x-y plane.

We start with finding the radiative transfer from an emitting slab labeled as j to a point z in a receiving slab γ, which will utilize Eq. (3). Based on relative positions of the slabs, the Weyl components in Eq. (3) need to be derived, which here relate the source point originated at z' in slab j with an observation point z in slab γ. Three scenarios can occur: 1, both slabs are in the left (hot) medium; 2, the two slabs are in separate medium; and 3, both are in the right (cold) medium. In all scenarios, we analyze the case that the emitter is located to the left of the receiver, and the reversed situation can be obtained from reciprocity. For derivation, the Green's function method [48] is used, and the Weyl tensor of electric field for slabs j and γ, $\overleftrightarrow{g}_E^{j\gamma}$, can be expressed as:

$$\overleftrightarrow{g}_E^{j\gamma}(\kappa, z, z', \omega) = \frac{i}{2} \frac{1}{k_{z,j}^q} \sum_{q=p,s} \tau_{j+1\to\gamma-1}^q \boldsymbol{E}_q^\gamma(z, \kappa) \otimes \boldsymbol{E}_q^j(z', \kappa) \tag{7}$$

Here we mainly discuss the second scenario, where $\tau_{j+1\to\gamma-1}^q$ represents the transmission of waves emanating from the surface of slab j, transmitting in medium 1 towards the vacuum gap ($\tau_{j+1\to m}^q$), across the vacuum gap (φ^q), and in medium 2 reaching the surface of slab γ ($\tau_{m+1\to\gamma-1}^q$), and is expressed as $\tau_{j+1\to m}^q \varphi^q \tau_{m+1\to\gamma-1}^q$. φ^q has the same expression as the transmission function in the two-body formalism, $\tau_{1\to2}^q$. m and $m+1$ are the slabs adjacent to the vacuum gap as shown in Fig. 1. $k_{z,j}^q$ is normal component of wave vector in slab j. $\boldsymbol{E}_q^j$ and $\boldsymbol{E}_q^\gamma$ are expressed as:

$$\boldsymbol{E}_q^j(z', \kappa) = \boldsymbol{e}_{q+}^j e^{ik_{z,j}^q (z_j - z')} \tag{8}$$

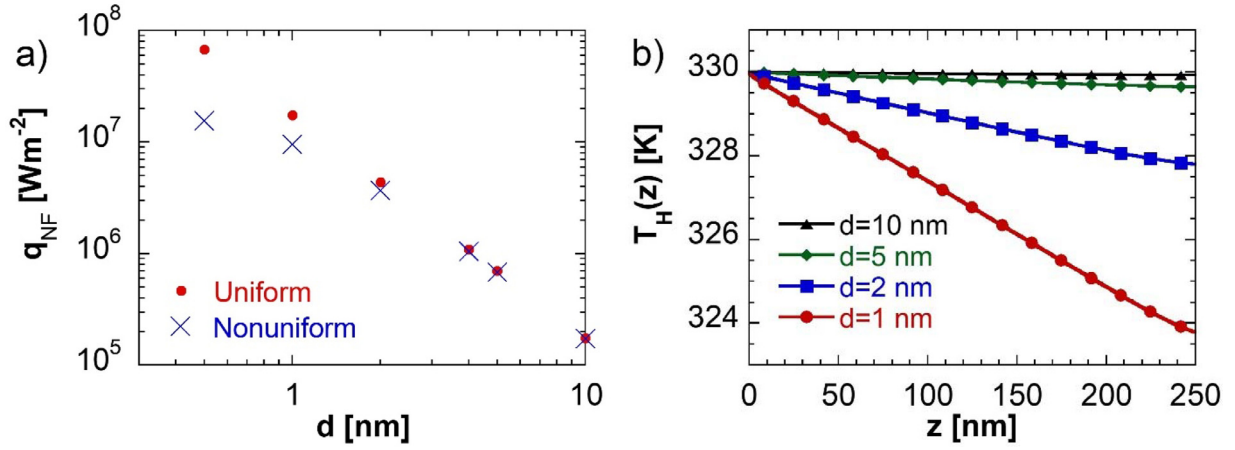$$\boldsymbol{E}_q^\gamma(z, \kappa) = \boldsymbol{e}_{q+}^\gamma e^{ik_{z,\gamma}^q (z-z_{\gamma-1})} \tag{9}$$

Eq. (8) represents right going wave originated from unit strength wave at z' and emerging from the boundary of the emitting slab (z_j, see Fig. 1). $\boldsymbol{E}_q^\gamma$ in Eq. (9) is the field of the right going wave originated from unit strength wave at $z_{\gamma-1}$ (the left boundary of slab γ) to z. Substituting Eqs. (8) and (9) into Eq. (7) results in the detailed expressions of the Weyl components, which are used to find the Poynting vector at an observation point z due to radiation from the emitting slab by integrating z' from z_{j-1} to z_j in Eq. (3). Expression of φ^q and the detailed Weyl components for the magnetic field are given in Supplemental Material S2.

To find the radiative heat flux from the emitter j to the receiver γ, we evaluate the difference in the Poynting vectors at the boundaries of slab γ, $z_{\gamma-1}$ and z_γ which can be expressed in a compact form as:

$$q_{j\to\gamma} = \int_0^\infty \frac{d\omega}{2\pi} (\langle S_z(z_{\gamma-1}, \omega)\rangle - \langle S_z(z_\gamma, \omega)\rangle)$$
$$= \int_0^\infty \frac{d\omega}{2\pi} \Theta(\omega, T_j) \int_{\omega/c}^{\kappa_{max}} \frac{d\kappa}{2\pi} \kappa \sum_{i=s,p} \mathcal{T}_q^{j,\gamma} \tag{10}$$

Similar to $\mathcal{T}_q^{1,2}$ in Eq. (1), we call $\mathcal{T}_q^{j,\gamma}$ energy exchange function. The final expression of $\mathcal{T}_q^{j,\gamma}$ for the second scenario is derived as:

$$\mathcal{T}_q^{j,\gamma} = \beta_q^j \left(1 - e^{-2Im(k_{z,j}^q)\delta_j}\right) \left\{ \left|\tau_{j+1\to m}^q\right|^2 |\varphi^q|^2 \left|\tau_{m+1\to\gamma-1}^q\right|^2 \right\}$$
$$\times \left(1 - e^{-2Im(k_{z,\gamma}^q)\delta_\gamma}\right) \beta_q^\gamma \tag{11}$$

Fig. 2. (a) Radiative heat transfer from the hot to cold medium with respect to vacuum separation for uniform and nonuniform temperature conditions. Results overlap for separation gaps greater than 5 nm. We note lower limit of logarithmic x-axis starts from 0.3. (b) The temperature profile across hot medium for $d = 10$ nm, 5 nm, 2 nm, and 1 nm.

The expressions for the first and third scenarios are given in Supplemental Material S3. Eq. (11) is the central result of the derived many-body formalism. The energy exchange function, $\mathcal{T}_q^{j,\gamma}$, represents the interaction of the emitter and the receiver for a given mode. Similar to $\mathcal{T}$ in the two-body formalism, $\mathcal{T}_q^{j,\gamma} \leq 1$. Emission of waves from slab j with thickness δ_j is given by $\beta_q^j(1 - e^{-2Im(k_{z,j})\delta_j})$. β_q^j is related to the out-of-plane wave vector k_z^q(see Supplemental Materials S4) and is a constant in either medium 1 or 2 owing to continuous media. The emitted waves interact with the receiver after transmitting through the slabs in medium 1, represented by $|\tau_{j+1\to m}^p|^2$ in Eq. (11), tunneling across the vacuum gap $|\varphi^q|^2$, traversing through the slabs in medium 2 $|\tau_{m+1\to\gamma-1}^q|^2$ and reaching the receiver. During the interaction with the receiver, waves are absorbed as $(1 - e^{-2Im(k_{z,\gamma}^q)\delta_\gamma})\beta_q^\gamma$. $|\varphi^q|^2$ represents the fraction of transmitted energy across the vacuum gap. It can be shown that $\beta_q|\varphi^q|^2\beta_q$ has exactly the same expression as Eq. (2) for evanescent waves (see Supplemental Materials S4). Lastly, it can be shown that the energy exchange function obeys reciprocity, i.e. $\mathcal{T}^{j,\gamma} = \mathcal{T}^{\gamma,j}$. Therefore, the expressions are valid when the emitter is located to the right of the receiver.

We can now write net radiative heat exchange between two slabs, j and γ as

$$q_{j,\gamma} = q_{j\to\gamma} - q_{\gamma\to j} = \int_0^\infty \frac{d\omega}{2\pi}\left[\Theta(\omega, T_j) - \Theta(\omega, T_\gamma)\right]\int_{\omega/c}^{\kappa_{max}}\frac{d\kappa}{2\pi}\kappa\mathcal{T}_q^{j,\gamma} \quad (12)$$

and the net radiative heat transfer into slab j, $q^{(j)}$, by summation over all slabs as

$$q^{(j)} = -\sum_{l\neq j}^N q_{j,l} = \sum_{l\neq j}^N q_{l,j}$$

$$= \int_0^\infty \frac{d\omega}{2\pi}\sum_{l\neq j}^N\left[\Theta(\omega, T_l) - \Theta(\omega, T_j)\right]\int_{\omega/c}^{\kappa_{max}}\frac{d\kappa}{2\pi}\kappa_q^{l,j} \quad (13)$$

Eq. (13) has a similar form as Eq. (1). To solve for the radiative heat transfer for given reservoir temperatures, we find the set of net radiative heat transfer $(q^{(1)}, q^{(2)}, \ldots, q^{(N)})$ and a temperature profile that yields $q^{(j)} = 0$ for the entire set except reservoirs (which can be done using an iterative procedure), then the global system reaches global equilibrium. The corresponding temperature profile in the media is unique to the state and is the global equilibrium temperature profile. In the computed set, $q^{(1)}(= -q^{(N)})$ represents the net radiative heat transfer between the hot and cold media, which is also the near-field radiative transfer between the

two media. The detailed solution procedure can be found in Ref. [49].

Our model is applicable to radiation between any type of material (metal, dielectric, artificial and natural hyperbolic material) across a vacuum gap. Limitation of the current model is the assumption of uniform dielectric properties within the media, which may not be valid if the length scale in some artificial (meta) materials is large. In addition, the current model neglects the temperature dependence of the optical properties within media.

3. Results and discussion

3.1. Many-body vs. two-body formalism

We first apply the many-body formalism derived above to the situation when the medium on each side of the gap has a uniform temperature. All slabs in hot and cold media are at their reservoir temperatures, T_H and T_C, respectively. From Eq. (12), it is seen that for slabs in the same medium, $q_{j,\gamma} = 0$. Thus, the net radiation is only transferred between slabs in separate media. To find net heat transfer from slab j in medium 1 to the entire medium 2, we calculate $\sum_{\gamma=m+1}^N q_{j,\gamma} = q_{j,cold}$. The net heat transfer from medium 1 to 2 is obtained by summing the net heat transfers, $q_{j,cold}$, for all slabs in medium 1, $q_{1,2} = \sum_{j=1}^m q_{j,cold} = \sum_{j=1}^m\sum_{\gamma=m+1}^N q_{j,\gamma}$. Owing to the uniform temperatures, the summation only needs to be applied to $\mathcal{T}_q^{j,\gamma}$, i.e., $\sum_{j=1}^m\sum_{\gamma=m+1}^N \mathcal{T}_q^{j,\gamma}$. Here, $\mathcal{T}_q^{j,\gamma}$ is expressed as Eq. (11) for the scenario that the two slabs are on different sides of the vacuum separation. The inner summation over γ for multiplication of $|\tau_{m+1\to\gamma}^q|^2$ with $(1 - e^{-2Im(k_{z,\gamma}^q)\delta_\gamma})$ in Eq. (11) yields 1. Similarly, the outer summation over j for multiplication of $|\tau_{j+1\to m}^q|^2$with $(1 - e^{-2Im(k_{z,j}^q)\delta_j})$ also results in 1. Hence, the summations reduce $\mathcal{T}_q^{j,\gamma}$ to $\beta_q|\varphi^q|^2\beta_q$, which is the same expression as the energy exchange function between two slabs with uniform temperature, and is the same expression as Eq. (2) as indicated previously (the proof is given in Supplemental Material S4). Therefore, we obtain the exact result of the two-body formalism. This shows the two-body formalism with uniform temperatures is simply a special case of the many-body formalism.

The many-body model reducing to the two-body model under uniform temperature condition indicates that the two formalisms consider phonon polaritons with the same origin for near-field radiative transfer, which depends on the probability of phonon po-
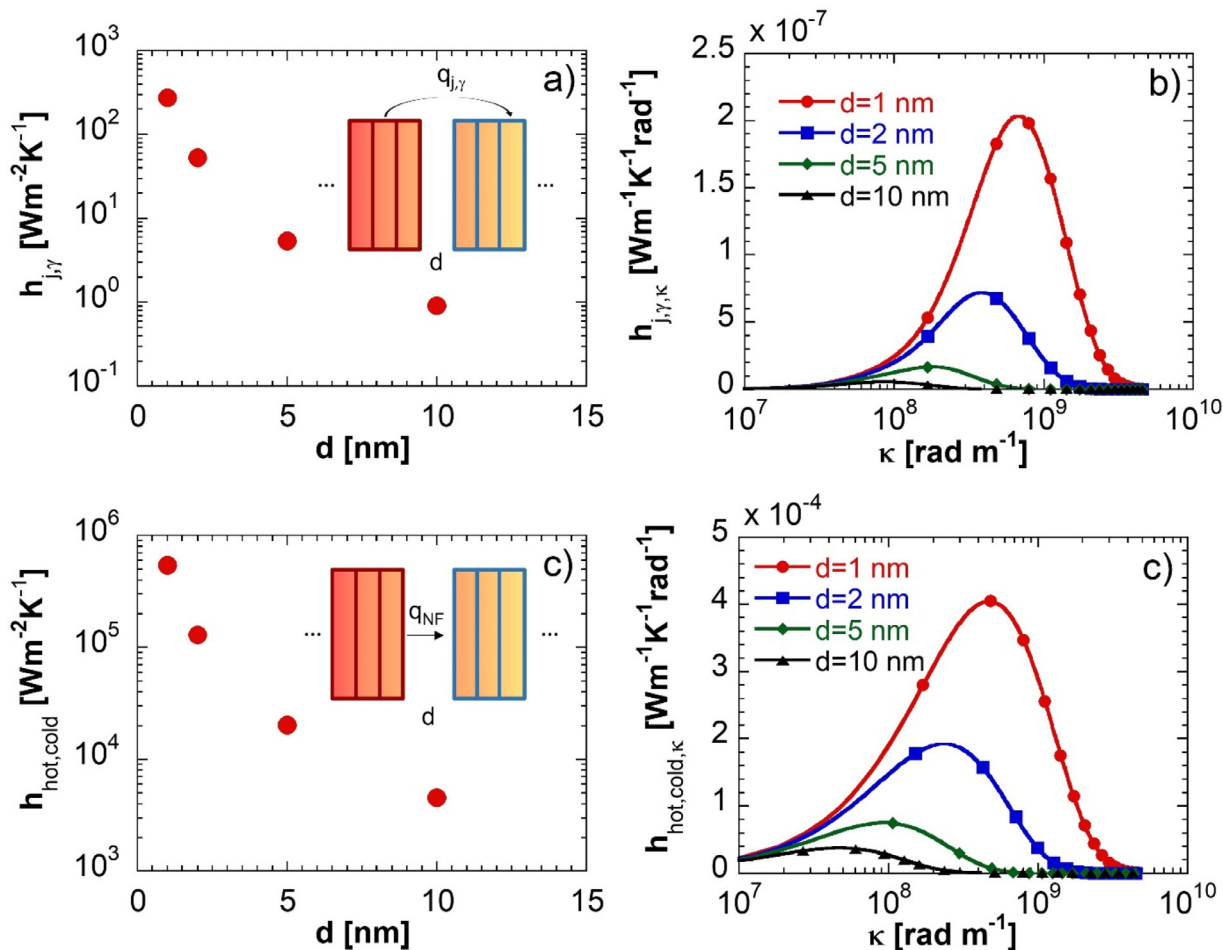
Fig. 3. (a) Heat transfer coefficient, as a measure of coupling strength, between two slabs located 5 nm away from the vacuum-material interface at opposite sides of the vacuum separation as a function of gap size. The slab thickness used for the calculations is 0.5 nm. (b) Wave vector dependent heat transfer coefficient for the corresponding gap sizes. The cutoff wavevector is 3.14×10^9, 1.57×10^9, 6.28×10^9, and 3.14×10^8 rad/m for $d = 1$ nm, 2 nm, 5 nm, and 10 nm, respectively. (c) Total heat transfer coefficient between hot and cold media as a function of gap size. (d) Wave vector dependent total heat transfer coefficient between two media for the corresponding gap sizes.

laritons tunneling across the vacuum gap. Although the two-body formalism is sometimes equivalated using a surface treatment [5], it in fact does not distinguish the origin of radiation. At uniform temperature, radiation is also generated from the bulk, but a wave removes a net amount of heat only when crossing the surface, whereas there is no net radiation exchange within each body with a uniform temperature. On the other hand, the many-body formalism accounts for the net radiation exchange via phonon polaritons within the same medium, as well as their contribution to the near-field radiative transfer across the gap.

3.2. Near-field radiation driven by temperature gradient

We first show the results of near-field radiative heat flux using the many-body approach. We consider a global system of 250-nm thick hexagonal boron nitride (hBN) films in contact with reservoirs at $T_H = 330$ K and $T_C = 300$ K and select 0.5-nm slab thickness throughout the study. We use dielectric properties of hBN from Ref. [40]. Fig. 2a shows the net radiative heat transfer, q_{NF}, from the hot to the cold medium with respect to d. The net radiative heat transfer increases with the decrease in d that allows HPhPs with larger wave vectors tunneling across the vacuum gap as seen from $e^{-2Im(k_{z,o})d}$ in Eq. (2). We also show the net radiative heat transfer, q_{NF}, calculated using the two-body formalism in Fig. 2a when hot and cold media are set at reservoir temperatures,

330 K and 300 K. Fig. 2a shows that q_{NF} for two-body and many-body approaches almost overlap for separations greater than 5 nm. This is because the temperatures are nearly uniform for the many-body formalism when the separation is large. Fig. 2b shows the temperature distributions in the hot medium for $d = 10$ nm, 5 nm, 2 nm, and 1 nm. The temperature profile or gradient is similar in the cold medium. We can see that for $d = 5$ nm and above, where q_{NF}s overlap in Fig. 2a, the temperature is nearly uniform. Note that the near-field radiation heat transfer is much greater than that of blackbody, which is ~210 Wm^{-2} between two surfaces at the same temperatures. Fig. 2a also shows q_{NF} from the many-body approach is less than that obtained using the two-body approach. This is because HPhP modes tunneling across the vacuum gap remove heat from the bulk, which leads to the temperature gradient and lower temperatures near the interface in the hot medium and higher temperature in the cold medium, resulting in a less amount of heat exchange.

Now we discuss in detail propagation of phonon polaritons driven by the temperature gradient across the vacuum gap. For this purpose, we consider a pair of slabs, with one in the hot medium and the other in the cold medium, each is positioned 5 nm away from the vacuum-material interface. Fig. 3a shows the heat transfer coefficient or the coupling strength between the pair of slabs, defined as $h_{j,\gamma} = \frac{q_{j,\gamma}}{T_j - T_\gamma}$, for different vacuum separations. The coupling between the slabs increases when the two media are brought
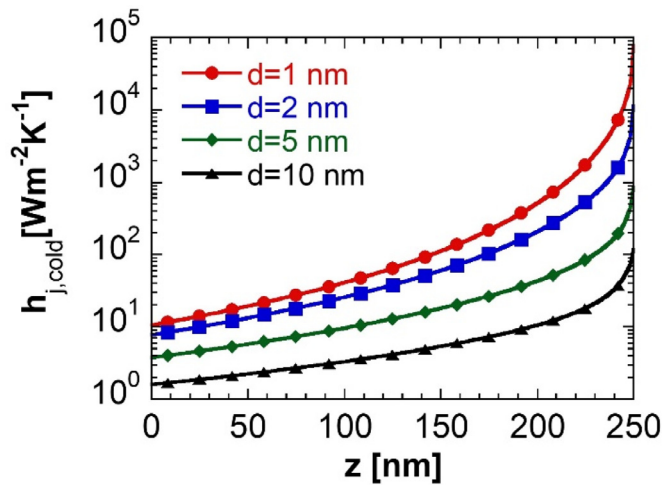
Fig. 4. Heat transfer coefficient of individual slabs with a thickness of 0.5 nm in the hot medium arising from interaction of the slab with the entire cold medium at vacuum separation of 1 nm, 5 nm, and 10 nm.

closer. This is explained by the wave vector dependent coupling strength shown in Fig. 3b. When the separation is decreased, the range of κ for tunneling polaritons increases. However, there is also a limit or cutoff for κ for each separation distance which is governed by the exponential decay in Eq. (2). This cutoff corresponds to $\kappa \sim (2d)^{-1}$, which is equivalent to total internal reflection. In addition to the increasing in range, the strength of coupling also increases when the gap is reduced due to the less attenuation of energy carried by a given wave vector across the gap as seen in Fig. 3b. When we compare coupling strengths for a given wave vector at different vacuum gaps, we also see the coupling strength enhances at shorter gap distances, which arises from less attenuation across the vacuum gap. Summation of $h_{j,\gamma}$ over j and γ, $\sum_{j=1}^{m} \sum_{\gamma=m+1}^{N} h_{j,\gamma}$, results in total heat transfer coefficient, $h_{hot,cold}$, between hot and cold media and is shown as a function of gap size in Fig. 3c. Comparison of Fig. 3a and c reveals similar trends of $h_{j,\gamma}$ and $h_{hot,cold}$ for the corresponding gap sizes. We also plot the wave vector-dependent total heat transfer coefficient, $h_{hot,cold,\kappa}$, in Fig. 3d. The trend of $h_{hot,cold,\kappa}$ is similar to that of $h_{j,\gamma,\kappa}$ in Fig. 3b for the corresponding gaps sizes due to cutoff of wave vectors corresponding to the gap size. We note that the peak heat transfer coefficient shifts toward larger wave vectors for smaller separations. We attribute this shift to the larger number of modes with large wave vectors confined in the same volume that carry energy.

Slabs near the interface have a stronger interaction with the medium across the vacuum gap than those farther away from the interface. We calculate $h_{j,cold} = \sum_{\gamma=m+1}^{N} h_{j,\gamma}$ where $h_{j,cold}$ represents the coupling strength of slab j in the hot medium with the entire cold medium. Fig. 4 shows $h_{j,cold}$ for all the slabs in the hot medium as a function of position of the slabs from the reservoir ($z = 0$ nm) for d = 10 nm, 5 nm, 2 nm and 1 nm. We see each individual slab contributes to the net radiative heat transfer from the hot to the cold medium. This is another indication that the origin of near-field heat transfer between hot and cold media is HPhPs generated within the bulk, even though the contribution by a slab decreases with distance away from the interface by orders of magnitude due to the short propagation lengths of the highly confined modes that contribute most to the near-field radiation transfer. Fig. 4 also shows that $h_{j,cold}$ increases with the decrease in the vacuum gap for all slabs due to less attenuation of the modes across the vacuum gap with shorter separation. The heat transfer

coefficient between two groups of slabs is calculated by summing the contributions from each pair, $h_{j,\gamma}$, in the groups.

Lastly, we note that this study considers only radiative transport as the heat transfer mechanism. Conduction also transports energy within a material. The many-body model can incorporate conduction during the temperature calculation and solve for local thermal equilibrium temperature by applying energy balance to each slab [44]. Additionally, conductive heat transfer across the vacuum gap can take place for sub-nm separations through phonon tunneling [50–53]. Even we have computed the near-field radiation effect with a separation below 1 nm (Fig. 2a), at that small gap phonon tunneling will likely need to be considered which will be the subject of another study.

4. Conclusion

To summarize, we have found that HPhPs responsible for energy transport across the vacuum gap between hyperbolic materials are bulk-originated polaritons. At uniform temperatures, the many-body approach that accounts for bulk-originated polaritons reduces to the two-body formalism, indicating the near-field radiative transfer described by the two-body formalism is just a special case of the many-body approach. When a temperature gradient exists in the media, HPhPs transfer net heat through the material as well as across the vacuum gap. Energy transfer across the vacuum gap is largely due to HPhPs with large wave vectors, which contribute even more to the enhanced near-field radiative transfer when the gap is reduced. Our model enables better prediction of near-field thermal radiation between hyperbolic materials. Applications of near-field radiation will require a precise control of the separation gap down to the nanometer level.

Declaration of Competing Interest

No competing interest is declared.

CRediT authorship contribution statement

Hakan Salihoglu: Conceptualization, Data curation, Methodology, Writing - original draft. **Xianfan Xu:** Conceptualization, Funding acquisition, Methodology, Supervision, Writing - review & editing.

Acknowledgment

Supplementary materials

Supplementary material associated with this article can be found, in the online version, at doi:10.1016/j.ijheatmasstransfer.2021.120984.

References

[1] M. Planck, The Theory of Heat Radiation, Dover Publications, Inc., 1991.
[2] D. Polder, M. Van Hove, Theory of radiative heat transfer between closely spaced bodies, Phys. Rev. B 4 (1971) 3303, doi:10.1103/PhysRevB.4.3303.
[3] J.J. Loomis, H.J. Maris, Theory of heat transfer by evanescent electromagnetic waves, Phys. Rev. B 50 (1994) 18517, doi:10.1103/PhysRevB.50.18517.
[4] S.M. Rytov, Y.A. Kravtsov, V.I. Tatarskii, Principles of Statistical Radiophysics, 3, 1987.
[5] J. Pendry, Radiative exchange of heat between nanostructures, J. Phys. Condens. Matter 11 (1999) 6621–6633, doi:10.1088/0953-8984/11/35/301.
[6] J.-P. Mulet, K. Joulain, R. Carminati, J.-J. Greffet, Enhanced radiative heat transfer at nanometric distances, Microscale Thermophys. Eng. 6 (2002) 209–222, doi:10.1080/10893950290053321.

[7] S. Shen, A. Narayanaswamy, G. Chen, Surface phonon polaritons mediated energy transfer between nanoscale gaps, Nano Lett. 9 (2009) 2909–2913, doi:10.1021/nl901208v.

[8] E. Rousseau, A. Siria, G. Jourdan, S. Volz, F. Comin, J. Chevrier, J.-J. Greffet, Radiative heat transfer at the nanoscale, Nat. Photonics 3 (2009) 514–517, doi:10.1038/nphoton.2009.144.

[9] R.S. Ottens, V. Quetschke, S. Wise, A.A. Alemi, R. Lundock, G. Mueller, D.H. Reitze, D.B. Tanner, B.F. Whiting, Near-field radiative heat transfer between macroscopic planar surfaces, Phys. Rev. Lett. 107 (2011) 014301, doi:10.1103/PhysRevLett.107.014301.

[10] B. Song, Y. Ganjeh, S. Sadat, D. Thompson, A. Fiorino, V. Fernández-Hurtado, J. Feist, F.J. Garcia-Vidal, J.C. Cuevas, P. Reddy, E. Meyhofer, Enhancement of near-field radiative heat transfer using polar dielectric thin films, Nat. Nanotechnol. 10 (2015) 253, doi:10.1038/NNANO.2015.6.

[11] K. Kim, B. Song, V. Fernández-Hurtado, W. Lee, W. Jeong, L. Cui, D. Thompson, J. Feist, M.T.H. Reid, F.J. García-Vidal, J.C. Cuevas, E. Meyhofer, P. Reddy, Radiative heat transfer in the extreme near field, Nature (2015) 528, doi:10.1038/nature16070.

[12] R. St-Gelais, L. Zhu, S. Fan, M. Lipson, Near-field radiative heat transfer between parallel structures in the deep subwavelength regime, Nat. Nanotechnol. 11 (2016) 515–519, doi:10.1038/NNANO.2016.20.

[13] A. Fiorino, D. Thompson, L. Zhu, B. Song, P. Reddy, E. Meyhofer, Giant enhancement in radiative heat transfer in sub-30 nm gaps of plane parallel surfaces, Nano Lett. 18 (2018) 3711–3715, doi:10.1021/acs.nanolett.8b00846.

[14] J. Desutter, L. Tang, M. Francoeur, A near-field radiative heat transfer device, Nat. Nanotechnol. 14 (2019) 751–755, doi:10.1038/s41565-019-0483-1.

[15] H. Salihoglu, W. Nam, L. Traverso, M. Segovia, P. Venuthurumilli, W. Liu, Y. Wei, W. Li, X. Xu, Near-field thermal radiation between two plates with sub-10 nm vacuum separation, Nano Lett. 20 (2020) 6091–6096, doi:10.1021/acs.nanolett.0c02137.

[16] C.R. Otey, W. Tung Lau, S. Fan, Thermal rectification through vacuum, Phys. Rev. Lett. 104 (2010), doi:10.1103/PhysRevLett.104.154301.

[17] J. Huang, Q. Li, Z. Zheng, Y. Xuan, Thermal rectification based on thermochromic materials, Int. J. Heat Mass Transf. 67 (2013) 575–580, doi:10.1016/j.ijheatmasstransfer.2013.08.057.

[18] P. Ben-Abdallah, Near-field thermal transistor, Phys. Rev. Lett. 112 (2014) 044301, doi:10.1103/PhysRevLett.112.044301.

[19] A. Fiorino, L. Zhu, D. Thompson, R. Mittapally, P. Reddy, E. Meyhofer, Nanogap near-field thermophotovoltaics, Nat. Nanotechnol. 13 (2018) 806–811, doi:10.1038/s41565-018-0172-5.

[20] A. Fiorino, D. Thompson, L. Zhu, R. Mittapally, S.-A. Biehs, O. Bezencenet, N. El-Bondry, S. Bansropun, P. Ben-Abdallah, E. Meyhofer, P. Reddy, A thermal diode based on nanoscale thermal radiation, ACS Nano 12 (2018) 5774–5779, doi:10.1021/acsnano.8b01645.

[21] J.-J. Greffet, R. Carminati, K. Joulain, J.-P. Mulet, S. Mainguy, Y. Chen, Coherent emission of light by thermal sources, Nature 416 (2002) 61–64, doi:10.1038/416061a.

[22] K. Joulain, J.-P. Mulet, F. Marquier, R. Carminati, J.-J. Greffet, Surface electromagnetic waves thermally excited: radiative heat transfer, coherence properties and Casimir forces revisited in the near field, Surf. Sci. Rep. 57 (2005) 59–112, doi:10.1016/j.surfrep.2004.12.002.

[23] R. St-Gelais, B. Guha, L. Zhu, S. Fan, M. Lipson, Demonstration of strong near-field radiative heat transfer between integrated nanostructures, Nano Lett. 14 (2014) 6971–6975, doi:10.1021/nl503236k.

[24] B. Song, D. Thompson, A. Fiorino, Y. Ganjeh, P. Reddy, E. Meyhofer, Radiative heat conductances between dielectric and metallic parallel plates with nanoscale gaps, Nat. Nanotechnol. 11 (2016) 509–514, doi:10.1038/NNANO.2016.17.

[25] J. Yang, W. Du, Y. Su, Y. Fu, S. Gong, S. He, Y. Ma, Observing of the super-Planckian near-field thermal radiation between graphene sheets, Nat. Commun. 9 (2018) 4033, doi:10.1038/s41467-018-06163-8.

[26] S.-A. Biehs, E. Rousseau, J.-J. Greffet, Mesoscopic description of radiative heat transfer at the nanoscale, Phys. Rev. Lett. 105 (2010) 234301, doi:10.1103/PhysRevLett.105.234301.

[27] X.L. Liu, R.Z. Zhang, Z.M. Zhang, Near-field radiative heat transfer with doped-silicon nanostructured metamaterials, Int. J. Heat Mass Transf. 73 (2014) 389–398, doi:10.1016/j.ijheatmasstransfer.2014.02.021.

[28] J. Shi, B. Liu, P. Li, L.Y. Ng, S. Shen, Near-field energy extraction with hyperbolic metamaterials, Nano Lett. 15 (2015) 1217–1221, doi:10.1021/nl504332t.

[29] M. Lim, J. Song, S.S. Lee, B.J. Lee, Tailoring near-field thermal radiation between metallo-dielectric multilayers using coupled surface plasmon polaritons, Nat. Commun. 9 (2018), doi:10.1038/s41467-018-06795-w.

[30] K. Shi, F. Bao, S. He, Enhanced near-field thermal radiation based on multilayer graphene-hBN heterostructures, ACS Photonics 4 (2017) 971–978, doi:10.1021/acsphotonics.7b00037.

[31] W. Du, J. Yang, S. Zhang, N. Iqbal, Y. Dang, J.-B. Xu, Y. Ma, Super-Planckian near-field heat transfer between hyperbolic metamaterials, Nano Energy 78 (2020) 105264, doi:10.1016/j.nanoen.2020.105264.

[32] J.Y. Chang, P. Sabbaghi, L. Wang, Near-field radiative heat transfer between nanowire-based dual uniaxial magneto-dielectric metamaterials, Int. J. Heat Mass Transf. 158 (2020) 120023, doi:10.1016/j.ijheatmasstransfer.2020.120023.

[33] Z. Jacob, I.I. Smolyaninov, E.E. Narimanov, Broadband Purcell effect: radiative decay engineering with metamaterials, Appl. Phys. Lett. 100 (2012) 181105, doi:10.1063/1.4710548.

[34] H.N.S. Krishnamoorthy, Z. Jacob, E. Narimanov, I. Kretzschmar, V.M. Menon, Topological transitions in metamaterials, Science (80-.) 336 (2012) 205–210, doi:10.1126/science.1219171.

[35] Z. Liu, H. Lee, Y. Xiong, C. Sun, X. Zhang, Far-field optical hyperlens magnifying sub-diffraction-limited objects, Science (80-.) 315 (2007) 1686, doi:10.1126/science.ll37368.

[36] J.S. Gomez-Diaz, A. Alù, Flatland optics with hyperbolic metasurfaces, ACS Photonics 3 (2016) 2211–2224, doi:10.1021/acsphotonics.6b00645.

[37] Y. Cui, K.H. Fung, J. Xu, H. Ma, Y. Jin, S. He, N.X. Fang, Ultrabroadband light absorption by a sawtooth anisotropic metamaterial slab, Nano Lett. 12 (2012) 1443–1447, doi:10.1021/nl204118h.

[38] A. Poddubny, I. Iorsh, P. Belov, Y. Kivshar, Hyperbolic metamaterials, Nat. Photonics 7 (2013) 958–967, doi:10.1038/nphoton.2013.243.

[39] E.E. Narimanov, A.V. Kildishev, Naturally hyperbolic, Nat. Photonics 9 (2015) 214–216, doi:10.1038/nphoton.2015.56.

[40] J.D. Caldwell, A.V Kretinin, Y. Chen, V. Giannini, M.M. Fogler, Y. Francescato, C.T. Ellis, J.G. Tischler, C.R. Woods, A.J. Giles, M. Hong, K. Watanabe, T. Taniguchi, S.A. Maier, K.S. Novoselov, Sub-diffractional volume-confined polaritons in the natural hyperbolic material hexagonal boron nitride, Nat. Commun. 5 (2014) 5221, doi:10.1038/ncomms6221.

[41] L.V Brown, M. Davanco, Z. Sun, A. Kretinin, Y. Chen, J.R. Matson, I. Vurgaftman, N. Sharac, A.J. Giles, M.M. Fogler, T. Taniguchi, K. Watanabe, K.S. Novoselov, S.A. Maier, A. Centrone, J.D. Caldwell, Nanoscale mapping and spectroscopy of nonradiative hyperbolic modes in hexagonal boron nitride nanostructures, Nano Lett. 18 (2018) 1628–1636, doi:10.1021/acs.nanolett.7b04476.

[42] Y. Guo, Z. Jacob, Thermal hyperbolic metamaterials, Opt. Express 21 (2013) 15014–15019, doi:10.1364/OE.21.015014.

[43] S.-A. Biehs, M. Tschikin, P. Ben-Abdallah, Hyperbolic metamaterials as an analog of a blackbody in the near field, Phys. Rev. Lett. 109 (2012) 104301, doi:10.1103/PhysRevLett.109.104301.

[44] H. Salihoglu, V. Iyer, T. Taniguchi, K. Watanabe, P.D. Ye, X. Xu, Energy transport by radiation in hyperbolic material comparable to conduction, Adv. Funct. Mater. 30 (2020) 6–11, doi:10.1002/adfm.201905830.

[45] K. Park, S. Basu, W.P. King, Z.M. Zhang, Performance analysis of near-field thermophotovoltaic devices considering absorption distribution, J. Quant. Spectrosc. Radiat. Transf. 109 (2008) 305–316, doi:10.1016/j.jqsrt.2007.08.022.

[46] Z. Zheng, Y. Xuan, Theory of near-field radiative heat transfer for stratified magnetic media, Int. J. Heat Mass Transf. 54 (2011) 1101–1110, doi:10.1016/j.ijheatmasstransfer.2010.11.012.

[47] M. Tschikin, S.-A. Biehs, P. Ben-Abdallah, S. Lang, A.Yu Petrov, M. Eich, Radiative heat flux predictions in hyperbolic metamaterials, J. Quant. Spectrosc. Radiat. Transf. 158 (2015) 17–26, doi:10.1016/j.jqsrt.2014.11.013.

[48] J.E. Sipe, New Green-function formalism for surface optics, J. Opt. Soc. Am. B 4 (1987) 481, doi:10.1364/JOSAB.4.000481.

[49] I. Latella, P. Ben-Abdallah, S.-A. Biehs, M. Antezza, R. Messina, Radiative heat transfer and nonequilibrium Casimir-Lifshitz force in many-body systems with planar geometry, Phys. Rev. B 95 (2017) 205404.

[50] Y. Ezzahri, K. Joulain, Vacuum-induced phonon transfer between two solid dielectric materials: Illustrating the case of Casimir force coupling, Phys. Rev. B 90 (2014) 115433, doi:10.1103/PhysRevB.90.115433.

[51] V. Chiloyan, J. Garg, K. Esfarjani, G. Chen, Transition from near-field thermal radiation to phonon heat conduction at sub-nanometre gaps, Nat. Commun. 6 (2015) 6755, doi:10.1038/ncomms7755.

[52] J. Pendry, K. Sasihithlu, R.V Craster, Phonon-assisted heat transfer between vacuum-separated surfaces, Phys. Rev. B 94 (2016) 75414, doi:10.1103/PhysRevB.94.075414.

[53] A.I. Volokitin, Contribution of the acoustic waves to near-field heat transfer, J. Phys. Condens. Matter. 32 (2020) 215001, doi:10.1088/1361-648X/ab71a5.